Efficient Herbicide Spray Pattern Generation for Site-Specific Weed Management Practices Using Semantic Segmentation on UAV Imagery

Beau Hobba[1], **Şafak Akıncı**[2], **Ali Haydar Göktoğan**[3],
The School of Aerospace, Mechanical and Mechatronic Engineering[1,3]
Australian Centre for Field Robotics[3], The University of Sydney, Australia[1,3]
hobbabeau@gmail.com[1], safakakinci17@gmail.com[2], a.goktogan@acfr.usyd.edu.au[3]

Abstract

Accurate detection of invasive weeds in sparse, rural regions is a significant challenge in Site-Specific Weed Management (SSWM). These weeds can be noxious to animals, downgrade the surrounding plants' standard of life, and cause a significant monetary deficit to farmers purchasing large quantities of herbicides. This paper uses semantic segmentation to detect, classify and geolocate common weeds: "Paterson's curse", "stinging nettle", "Scotch thistle" and "capeweed" in aerial imagery acquired by a Unmanned Aerial Vehicle (UAV). Finally, "herbicide maps" promoting SSWM are generated, providing farmers with tools to optimise the quantity of herbicide application, and the overall system has been successfully exploited in a 50-acre farm in Barwang, New South Wales (NSW), Australia.

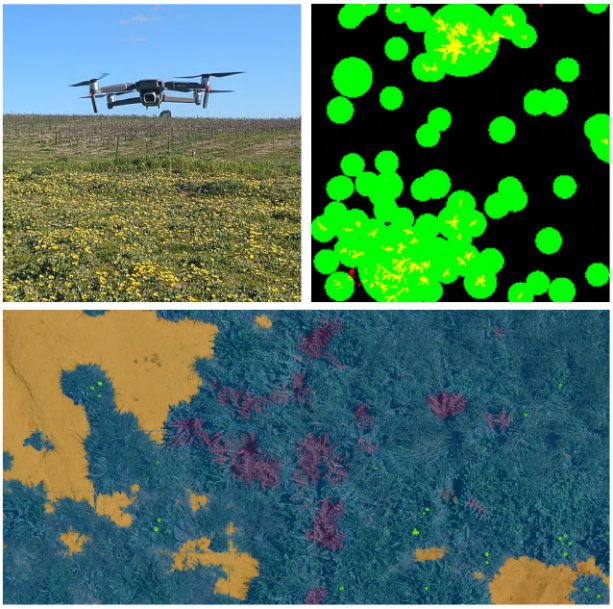

Figure 1: Aerial UAV imagery uses Semantic Segmentation to generate efficient herbicide spray patterns for SSWM.

1 Introduction

This paper presents a Deep Learning (DL)-based approach to perform semantic segmentation on aerial imagery of a rural area to detect and map weed infestations. Australian agriculture is shifting to a precision agriculture model as farmers use technological advancements to improve accuracy, efficiency and safety [Zhang *et al.*, 2017]. The proclaimed "Technology Tsunami" [Wu *et al.*, 2019] is perpetuated by the increase of Unmanned Aerial Vehicle (UAV) surveillance of crops, using Global Positioning System (GPS) technology for crop management, automatic tractors for crop harvest, and the modelling of weather to correspond with sowing. There is a strong incentive behind business developments in this new sector in the agriculture market.

The presented approach explicitly centred around the UAV usage for invasive weed monitoring. 61% of Australia's landmass is used for agriculture. Of this landmass, 7% is covered by invasive weeds [McLeod, 2018], which account for 5 billion Australian Dollar (AUD) per annum in lost production and control costs [McLeod, 2018], as large volumes of herbicide are required in animal grazing industries. There is a clear need for a solution to this monetary loss. These weeds can be noxious to animals and can downgrade the standard of life of surrounding plants, posing a significant problem for rural farms. Weeds can be present in crops such as wheat and rice fields and rural environments, such as sheep grazing land or general multi-purpose paddocks.

For a weed to be detected and classified, visual detection must be performed. Then farmers typically spray herbicide either on entire fields using tractors or single-handedly on individual weeds. This process is time-consuming, costly with all the herbicide applied to non-weeds, and damaging to the environment. The motivation behind using a UAV is that it provides imagery quickly due to being unobstructed in the air and can travel large areas in little time.

Farmers can opt for Site-Specific Weed Management

(a) Capeweed, *Arctotheca calendula* (b) Scotch thistle, *Onopordum acanthium* (c) Paterson's curse, *Echium plantagineum* (d) Stinging nettle, *Urtica incisa*

Figure 2: Close-up photographs of the invasive weeds to be detected with the UAV.

(SSWM). A notable portion of the cost of herbicide used can be saved by targeting only weed-specific locations. SSWM has the potential to reduce herbicide usage by up to 80% [Heap and Trengove, 2008], significantly reducing the $5 billion spent on agriculture each year [McLeod, 2018].

There is a wide variety of publications in the literature on the use of UAV aerial imagery for environmental purposes, including Pine Processionary Moth (PPM) infestations [Şafak Akıncı and Göktoğan, 2019], aquatic [Göktoğan *et al.*, 2010] or land-based weed infestations and assessment of weeds [Göktoğan and Sukkarieh, 2015]. For example, the system presented in [Rasmussen *et al.*, 2019] utilises Red Green Blue (RGB) cameras and a "thistle tool" to perform weed detection. Image processing techniques are used to remove crops from the image, such that DL can identify the remaining weeds. The system in [Louargant *et al.*, 2017] classifies between monocotyledonous and dicotyledonous plants. It uses machine learning on a laboratory-created database of plant and soil reflectance spectra. In most systems, the primary approach for weed detection is to create large orthomosaics of collected images, divide this into smaller sections and then extract the invasive weeds through segmentation [Göktoğan *et al.*, 2010] [Sa *et al.*, 2018]. It is also prevalent for these segmentations to use multispectral data and create specific vegetation based indices [Sa *et al.*, 2018].

1.1 Weeds as an Environmental Threat

Capeweed, *Arctotheca calendula*, shown in Figure 2a, quickly occupies large areas, dominating all other plants. Such infestations potentially reduce crop yield and revenue [Llewellyn *et al.*, 2016]. Additionally, capeweed is known as a nitrate accumulator, which can lead to nitrate poisoning when consumed by animals.

Scotch thistle, *Onopordum acanthium*, shown in Figure 2b, can injure animals and humans who walk near or on the plant and can render animal wool unusable. If not controlled, it will slowly overrun areas, especially since animals do not eat it [Briese, 2012]. Thus, it is solely a harmful weed.

Paterson's curse, *Echium plantagineum*, shown in Figure 2c, can easily spread due to its ability to create large quantities of seeds. It is toxic to livestock (especially horses and pigs), will infest common crops such as hay and grain, will overcrowd native vegetation, and commonly cause skin irritation to humans. It is also one of the most costly weeds in Australia [Sheppard and Smyth, 2012].

An unmaintained field of stinging nettle, *Urtica incisa*, will potentially produce reduced yields by up to 40 % [Coleman *et al.*, 2018]. The leaves and stem bare many microscopic hairs containing trichomes, fine, 'needle-like' hairs that inject several chemicals when touched. These nettles produce a painful sting and rash, which remains active in humans and livestock for many hours. The flowers of these plants also contribute strongly to hay fever.

1.2 Motivation and the Proposed System

The primary motivation of this paper is to create a method of weed detection that highlights the need for precision agriculture by allowing for eradication to focus on specific sites instead of whole areas. Mapping these weeds into an interactive platform will make further discovery and actions more accessible. It will aid both scientists and farmers in their plights to remove invasive weeds from rural areas. Making detection, classification and mapping manageable on large areas will assist in creating a viable solution to the problems invasive weeds create in rural environments.

We propose a system that does not examine one specific invasive weed and can be used in landscapes other than crop fields. It will follow a procedure of semantic segmentation to classify weeds from the environment, herbicide maps to optimise predictions, frame correlation to convert classified weed locations to geolocations, and geographic mapping for visualisation. Figure 3 illustrates the pipeline of the proposed system.

The rest of this paper is organised to follow the workflow shown in Figure 3. Section 2 explains the data acquisition process. Section 4 presents the deep learning pipeline and semantic segmentation framework to detect the weeds in UAV imagery. Section 5 and Section 5.2 explains georeferencing of the detected weeds and Site-Specific Weed Management respectively. Finally, Section 7 draws a conclusion.

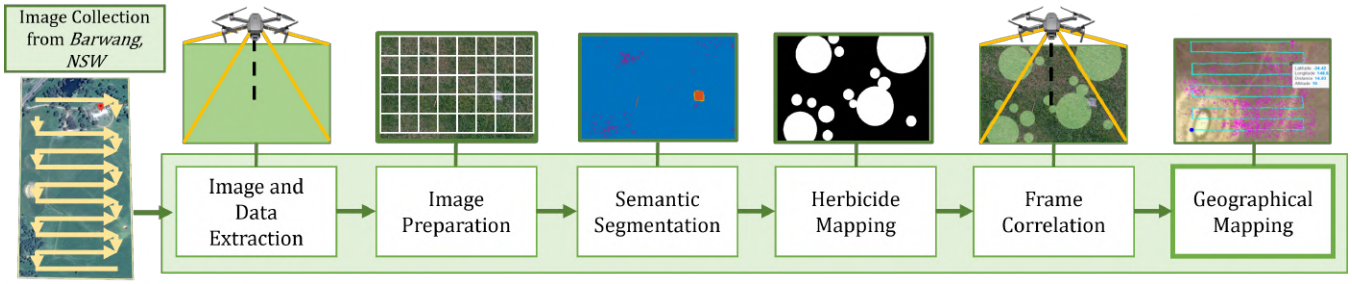

Figure 3: Workflow diagram of the proposed system.

2 Image and Data Extraction

The study site was located at *Shepherds Moon*, a 50-acre farm in Barwang, NSW, Australia (coordinates 34° 24' 52.7" S, 148° 27'41.1" E, datum WGS84). Field surveys commenced from Autumn to Spring 2020. During this time, vegetation was especially prominent, with herbicide treatment being recommended on the surveyed sites.

Civil Aviation Safety Authority (CASA) flight rules, guidelines and standards adhered to during data collection. A flight height of 10 m was determined as the altitude for the UAV as it provides a high-resolution image where the small weed can be observed while a significant area of farmland can be mapped.

More than 2560 RGB images were collected over the planned flight paths with the Da-Jiang Innovations (DJI) Mavic 2 Pro UAV using the onboard Hasselblad L1D-20c camera with the resolution of 5472 x 3648 pixels for the raw imagery.

Data Acquisition

The UAV records a flight log whilst surveying the rural areas. This log provides a time-series array of various parameters, including latitude, longitude, yaw, pitch, roll and speed.

Geographical Location

The Coordinate Reference Frame (CRF) of the UAV is determined to perform localisation of each weed and to account for the UAV position. The world position, represented by w, of the UAV is considered as the geographical latitude and longitude of the takeoff location; this point corresponds to $(0,0,0)$ in the coordinate axes and is represented by ${}^{w}\mathbf{P}$.

The inertial reference frame of the UAV uses the stationary Earth as its reference point and is represented by ${}^{UAV}\mathbf{P}$. This value uses the North East Down (NED) frame classification system, as demonstrated in Figure 4.

An Euler rotation matrix is used to model the yaw, pitch and roll of the UAV. This allows rotations to be represented about the coordinate axes by the angles ψ, θ and ϕ:

$$ {}^{w}_{UAV}\mathbf{R} = \mathbf{R}_z(\psi)\mathbf{R}_y(\theta)\mathbf{R}_x(\phi) \tag{1} $$

The UAV experiences external rotations based on factors such as wind. The position of the UAV with accordance to w is represented by the transformation equation ${}^{w}_{UAV}\mathbf{T}$, expressed in Equation 2.

The transformation of the UAV gimbal, denoted as g, is found with respect to the UAV; represented in Equation 3. g is rotated to face the ground directly below, and thus the rotation between g and the UAV is 0°. The gimbal's position, ${}^{g}\mathbf{P}$ is the distance from g to the UAV.

$$ {}^{w}_{UAV}\mathbf{T} = {}^{w}\mathbf{P} + {}^{w}_{UAV}\mathbf{R}\,{}^{UAV}\mathbf{P} \tag{2} $$

$$ {}^{UAV}_{g}\mathbf{T} = {}^{UAV}\mathbf{P} + {}^{g}\mathbf{P} \tag{3} $$

The transformation of the UAV camera, denoted as c, is found with respect to g; represented in Equation 4. The camera's position, ${}^{g}\mathbf{P}$ is the distance from c to g, represented by ${}^{c}\mathbf{P}$. The position of a weed, represented by ${}^{weed}\mathbf{P}$, is calculated with respect to c, represented in Equation 5.

$$ {}^{g}_{c}\mathbf{T} = {}^{g}\mathbf{P} + {}^{g}_{c}\mathbf{R}\,{}^{c}\mathbf{P} \tag{4} $$

$$ {}^{c}_{weed}\mathbf{T} = {}^{c}\mathbf{P} + {}^{weed}\mathbf{P} \tag{5} $$

The relation between w and a weed position is the summation of the previous transformations, as shown in Equation 6:

$$ {}^{w}_{weed}\mathbf{T} = {}^{c}_{weed}\mathbf{T}\,{}^{g}_{c}\mathbf{T}\,{}^{UAV}_{g}\mathbf{T}\,{}^{w}_{UAV}\mathbf{T} \tag{6} $$

The location of each weed is determined through the Ground Sample Distance (GSD), a method commonly used [Pflanz *et al.*, 2018],[Tan and Li, 2019] in UAV aerial imagery. This method converts 1 pixel to a physical distance and is demonstrated in Equation 7,

$$ GSD = \frac{S * h_t}{f * res_u} = 0.0022367 \text{ pixel/m} \tag{7} $$

where S is the sensor dimensions (mm), res_u is the image resolution width (pixel), h_t is the true altitude (m), and f is the focal length (mm). The conversion of the UAV image to a distance in m is useful for determining the location of the UAV and weeds in the real-world environment.

The image resolution pixels are converted to metres, where res_u is the image resolution width, res_v is the image resolution height and l is length of the resolutions (m)

$$ l_x = res_u \cdot GSD = 12.24 \text{ m} \qquad l_y = res_v \cdot GSD = 8.15 \text{ m} \tag{8} $$

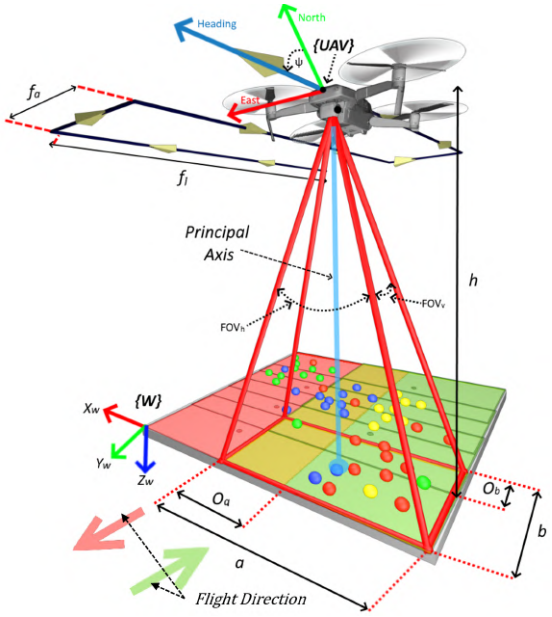

Figure 4: The geometry of the vertical aerial imagery acquired by a UAV camera pointing straight down.

The principal axis, pa, is the midpoint of the camera and the centre of the image plane. pa changes according to the rotation of the UAV and the gimbal. Due to g_{pitch} being directly aligned with with the UAV body frame, any external forces, such as wind, will change this axis. In perfect conditions, it will correspond to h_{total} (10 m). It is unlikely to assume zero external disturbance, and thus, the true altitude, h_{true}, is dependent on Equation 9.

$$h_{true} = \frac{h_{total}}{\cos\theta \cos\psi} \tag{9}$$

The pa coordinates correspond to a translation of h_{true} from c. As c is pointing directly at the ground, this translation is only in one direction. The transformation relates the UAV and the c image plane together, providing the pa coordinates, as determined in Equation 10.

Substituting these pa coordinates into the transformation of Equation 6 determines the principal point (middle) of the camera. As expressed in Equation 11, these points correspond to the x and y axes, as z is ground level (0 m).

$$^{weed}\mathbf{P} = \begin{bmatrix} h_{true} \\ 0 \\ 0 \end{bmatrix} \tag{10}$$

$$^{w}_{weed}\mathbf{P} = \begin{bmatrix} pa_x \\ pa_y \\ pa_z \approx 0 \end{bmatrix} \tag{11}$$

To find a real-world location (m), denoted as L_w and L_h, of a weed in an image, the weed's position in the image plane, denoted as L_u and L_v, is converted:

$$L_w = GSD * L_u \qquad L_l = GSD * L_v \tag{12}$$

The coordinate is then localised to the image resolution's perimeters solved in Equation 8. This yields the relationship between the weed object in the image and the UAV.

$$^{Weed_{uv}}\mathbf{P} = \begin{bmatrix} 0 \\ \frac{l_x}{2} - L_w \\ \frac{l_y}{2} - L_l \end{bmatrix} \tag{13}$$

The position of the weed is a translation from the previous pa coordinates. There is no rotation, as the UAV camera angle has not changed.

$$^{Weed}_{Weed_{uv}}\mathbf{T} = {}^{Weed_{uv}}\mathbf{P} \tag{14}$$

The final transformation relates back to the world reference frame. This is performed by implementing Equation 6. Now the position of each weed in the inertial frame can be determined and geographically tagged.

$$^{w}_{Weed_{uv}}\mathbf{P} = {}^{w}_{Weed}\mathbf{T}\,{}^{Weed}_{Weed_{uv}}\mathbf{T} \tag{15}$$

The position of the UAV regarding a global location is found through the consideration of latitude and longitude. An Earth-Centered, Earth-Fixed (ECEF) frame is established, where the X, Y and Z Cartesian coordinates of the UAV are configured concerning the centre of the Earth's mass, using the World Geodetic System (WGS) 84 as the world geodetic system. Thus, by corresponding the final distance values in metres found using CRF and GSD, these values can be converted to latitude and longitude values within the ECEF frame, as expressed in Equation 16.

$$M = \frac{1}{((2 \cdot \pi/360) \cdot r_{earth} \cdot 1000)} \tag{16}$$

where r_{earth} is 6378.137 km. A reference latitude, λE_{ref}, and longitude, λE_{ref}, is required to find new points.

$$\lambda E_{new} = \lambda E_{ref} + \Delta X \cdot M \qquad \phi E_{new} = \frac{\phi E_{ref} - (\Delta Y \cdot M)}{cos(\lambda E_{ref} \cdot (\pi/180))} \tag{17}$$

λE_{new} and ϕE_{new} correspond to a new geographic location, λE_{ref} and ϕE_{ref} is a reference location, and ΔX and ΔY are distance displacements in (m).

The UAV followed a waypoint system as demonstrated in Figure 4, when it flew parallel lines across the rural areas. Each waypoint consisted of a latitude, longitude and altitude coordinate. A reference location and the world position are defined to find the position of a new waypoint. The reference frame is the current latitude, longitude and altitude of the UAV when it obtains a photo. As the UAV flies according to set waypoints, each flight distance from the previous waypoint is represented by a and b, corresponding to the direction of travel. During these flights, the altitude remained consistent at 10 m. To ensure every location was sufficiently imaged, there was a region of overlap

referred to as O_a (40%) and O_b (60%). Waypoints related to longitude are denoted as w_b, and w_a for latitude. Reference waypoints are calculated in Equation 18.

$$w_{b_1} = \phi E_{ref} \qquad w_{a_1} = \lambda E_{ref} \tag{18}$$

The overlap region in metres is defined as:

$$o_\beta = res_v \cdot GSD \cdot o_v \qquad o_\alpha = res_u \cdot GSD \cdot o_u \tag{19}$$

and the displacement of the UAV in its directional flights:

$$b = (res_v \cdot GSD) - o_b \qquad \alpha = (res_u \cdot GSD) - o_\alpha \tag{20}$$

The next waypoint is then determined using Equation 17, resulting in:

$$w_{b_2} = w_{a_1} + \alpha * M \qquad w_{a_2} = \frac{w_{b_1} - (b \cdot M)}{cos(w_{a_1} \cdot (\pi/180))} \tag{21}$$

3 Image Preparation

For high throughput Convolutional Neural Network (CNN) operation on the Graphics Processing Units (GPUs), each original UAV image of size 5472 x 3648 pixels is split into squares of 224 x 224 pixels.

Image Labeling

Full resolution aerial images were annotated with the MATLAB labelling tool: Image Labeler. Nine classes were to be identified through the semantic segmentation network, including grass, Scotch thistle, Paterson's curse, stinging nettle, capeweed, water, dirt, dead thistle and others. As the class names are long, grass has been abbreviated to *GR*, Scotch thistle to *TH*, Paterson's curse to *PC*, stinging nettle to *SN*, and capeweed to *CW*. The four classes of water, dirt, dead scotch thistle and others are abbreviated as *OT*.

4 Semantic Segmentation

Semantic segmentation was used to detect weeds within the UAV imagery. We used Unet and SegNet architecture for image segmentation; with these models showing good performance for the detection of small objects [Şafak Akıncı and Göktoğan, 2019],[Asad and Bais, 2019]. We trained Unet and SegNet with different backbones, where ResNet50 gave the best scores for our dataset as demonstrated in Table 1. Figure 5 shows sample results from ResNet50. Class-wise classifications are evaluated as it is only appropriate to evaluate the four, weed classes.

Data Split

Each split image and the corresponding annotation were randomly shuffled and then split into groups of 70% training, 20% validation and 10% testing. There are 24,692 images and annotations for training, 7055 for validation, and a further 3527 for testing.

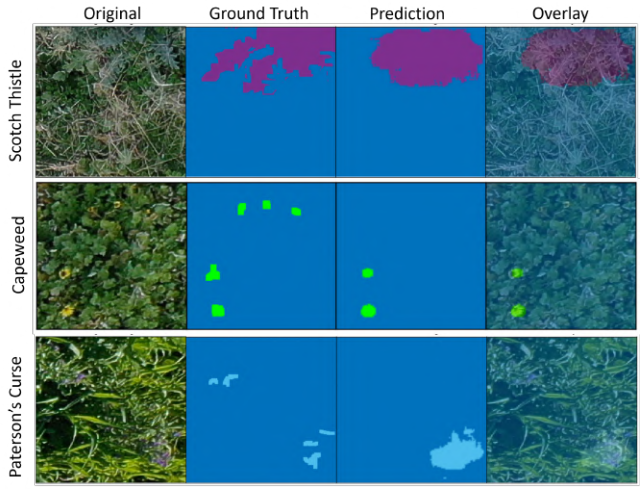

Figure 5: Predictions generated from the ResNet50-SegNet model on weeds.

Data Augmentation

Positional augmentation was used, which includes image transformations such as rotation, scaling and cropping. Colour augmentation on properties such as contrast, brightness, and saturation was also applied to both images and their respective segmentations.

Evaluation Metrics

Four evaluation metrics will be used, including precision, recall, F1-score and Intersection over Union (IoU). These are commonly used metrics in agriculture-based semantic segmentation projects [Şafak Akıncı and Göktoğan, 2019] [Milioto *et al.*, 2017].

Loss Functions

For training on the model, Focal Loss (FL) [Lin *et al.*, 2017] will be utilised. Contrary to Categorical Crossentropy Loss (CCE), FL takes into account the class imbalance.

Training

The training was performed using nine classes and an input image size of 224 x 224 pixels. The model's hyperparameters included setting the batch size to 64 and the number of epochs to 40. The optimiser used was Adagrad which provided an optimised gradient descent based on the learning parameters of each time-based iteration. The initial learning rate was set to 0.00032, with a callback to reduce the learning rate when the training process' loss plateaus for 10 epochs.

Prediction Results and Discussion

The model results represent the ResNet50-SegNet model, highlighted in green in Table 1, as the most effective at detecting and classifying weed classes. The model has the highest precision, recall, F1 score and IoU score in the detection of Scotch thistle and Paterson's curse. Although the

Table 1: Precision, Recall, F1-Score and IoU performance of the models and segmentation results for classes

	Precision (%)							**Recall (%)**						
	GR	*TH*	*PC*	*SN*	*CW*	*OT*	***Mean***	*GR*	*TH*	*PC*	*SN*	*CW*	*OT*	***Mean***
MobileNet-UNet	96.39	51.69	69.34	69.46	69.52	56.78	68.86	98.66	14.83	35.80	50.59	62.17	34.30	49.39
MobileNet-SegNet	96.35	48.63	70.21	72.00	59.22	57.11	67.25	98.68	14.75	35.59	49.57	51.57	29.25	46.57
ResNet50-Unet	96.95	40.27	74.39	71.43	**82.02**	53.72	69.79	98.73	6.76	48.20	**62.53**	45.69	22.86	47.46
ResNet50-SegNet	**97.30**	55.64	**77.09**	73.20	68.25	**68.84**	**73.39**	98.47	**29.76**	**58.04**	60.98	60.70	**51.07**	**59.84**
VGG16-Unet	94.68	0.00	0.00	43.50	16.67	28.95	30.63	**99.49**	0.00	0.00	0.07	0.00	18.39	19.66
VGG16-SegNet	96.96	**59.11**	73.81	**76.59**	67.02	58.75	72.04	98.64	25.90	50.99	56.33	60.66	39.27	55.30
	F1-Score (%)							**IoU (%)**						
MobileNet-UNet	97.51	23.05	47.22	58.54	**65.64**	41.26	55.54	95.14	13.02	30.91	41.38	48.85	30.77	43.35
MobileNet-SegNet	97.50	22.64	47.23	58.71	55.13	34.96	52.70	95.12	12.76	30.92	41.56	38.06	26.07	40.75
ResNet50-Unet	97.83	11.58	58.50	**66.68**	58.69	24.68	52.99	95.75	6.15	41.34	**50.02**	41.53	20.38	42.53
ResNet50-SegNet	**97.89**	**38.78**	**66.23**	66.54	64.25	**54.12**	**64.63**	**95.86**	**24.05**	**49.51**	49.85	**47.33**	**43.05**	**51.61**
VGG16-Unet	97.03	0.00	0.00	0.15	0.00	19.99	19.53	94.23	0.00	0.00	0.07	0.00	16.64	18.49
VGG16-SegNet	97.80	36.02	60.31	64.92	63.68	45.15	61.31	95.69	21.97	43.18	48.06	46.72	34.23	48.30

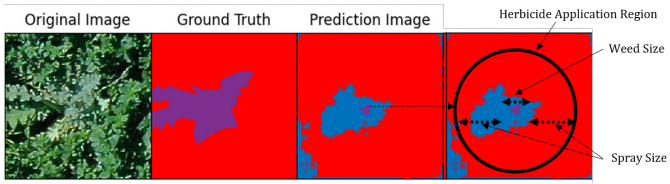

Figure 6: Predictions eventually can be developed to ensure the herbicide map performs full dispersion of herbicide.

results for the weed detection are relatively low, the prediction results show that the model can generalise the pixels related to weeds and provide a visually satisfactory prediction image. The reason for lower scores is the difficulty in labelling small weed objects in images and the sizeable imbalanced nature of the dataset. Additionally, although loss functions are used, grass still accounts for more than 90% of the data, and it is expected to still be the dominant class due to its non-unique shape and generally similar colour. The model successfully predicted differing weeds in an image with a clear focus on the pixels' detection and precision instead of the weed's accuracy and shape.

5 Herbicide Mapping

Herbicide maps are the creation of maps that detect regions where herbicide should be applied. These maps aim to achieve SSWM by reducing spray usage, ultimately saving the user both costs and time due to reduced refilling. Moreover, the reduction of herbicide leads to a positive effect on the environment [Shaw, 2005]. Herbicide maps are dictated by the semantic input prediction, the sprayer size and the characteristics of the weeds being managed. This is illustrated in Figure 6. Finally, a geographic map of each weed's location is created through geotagging 'spray regions' within the herbicide map.

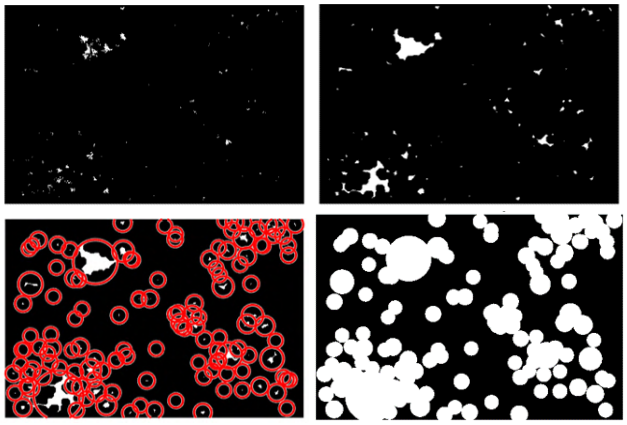

Figure 7: The creation of herbicide maps involves a process of enhancing the prediction and then finding the weeds based off of the mask. From top left to right: the segmentation mask, morphological processing, region detection and the final herbicide map mask.

Segmentation Mask

A semantic segmentation image prediction is converted from a RGB image to a Black, White (BW) mask. The prediction is generated from the semantic segmentation results. Only pixels related to the weeds are obtained, and each irrelevant class is removed. This mask is demonstrated in Figure 7.

Morphological Processing

Morphological operations, including erosion and dilation, are applied to the segmentation mask, yielding Figure 7.

$$A \cdot B = (A \oplus B) \ominus B \tag{22}$$

where, A represents the structuring element, B is the mask, $\oplus$ represents the dilation, and $\ominus$ represents the erosion.

This operation allows any weed clusters to be joined together whilst single weeds remain in their regular location.

The ideal size of the morphological close radius was obtained through testing the accuracy, efficiency and saved herbicide on a dataset of fifteen random images. As the structuring element increases in size, the weeds become clustered entirely together. Larger cluster sizes correlate to more herbicide required for eradication and ultimately a stable reduction in herbicide saved. The ideal closing radius occurs at 40 pixels, as found in these trials.

Spray Size

The width of the application herbicide spray is measured and considered as the swath width, denoted by S. This is the width created from spraying the weed at a direction perpendicular to the nozzle [Jensen *et al.*, 2013] and is calculated using Equation 23. S equates to 0.4 m, where the height of the spray, h, was estimated to be 0.2 m based off of the spray nozzle guide and weed size listed in [Tian *et al.*, 2000], where the angle, θ, is 0°.

$$S = 2 * h \tan(\frac{\theta}{2}) = 0.4 \text{ m} \tag{23}$$

Region Detection

Region detection uses the morphological mask as its input. It selects each morphological cluster in the mask by finding the masked regions' x and y centroid. x corresponds to the horizontal coordinate and y to the vertical coordinate. Next, each region's major and minor axis lengths are found, converting the region into an elliptical shape. The major axis, denoted by c, is represented by the maxima points connecting the two vertices of the ellipse, whilst the minor axis, denoted by d, is the minima points connected to the co-vertices of the ellipse. Equation 24 details the length of these points.

$$l_c = |c_\vee - c_\wedge|, \quad l_d = |d_\vee - d_\wedge| \tag{24}$$

Spray size, denoted by S, is converted from a real-life measurement (m) to a pixel-based measurement (S_{pixel}). The radius of the final region, denoted by r_{region}, is equivalent to half the horizontal and vertical diameters, denoted by $\varnothing$, with the addition of the spray width:

$$S_{pixel} = \frac{S}{GSD}, \quad \varnothing_i = [l_c, l_d]_i, \quad r_{region_i} = \frac{\varnothing_i}{2} + S_{pi} \tag{25}$$

where i represents the cluster/region. In Figure 7, the combination of these regions are marked as red circles.

Herbicide Map Mask

The circular regions are combined into the mask, as demonstrated in Figure 7. This final mask represents the herbicide map, denoted as H. The masked regions represent areas that must be managed, whilst the black represents areas that require no herbicide. Compared to traditional methods of spraying the entire field, this represents a significant improvement in reducing herbicide usage.

5.1 Herbicide Maps

Geographic mapping is used to represent the location of each weed. This real-world depiction validates the original location of the image and demonstrates the simplicity of converting this model to any real-world GPS tracking devices, such as tractors or other UAVs. The real-world map is also an interactive tool that farmers can use to see the density of weeds with respect to an imagery location. The reference world coordinate system is WGS84 to ensure consistency between the coordinate points and the transform calculations.

Using the proposed system, it is possible to perform observations over vast areas of forests in rapid succession using UAV imagery and deep learning.

5.2 Site-Specific Weed Management

SSWM in large areas is a difficult task. Weeds can be fought mechanically and chemically. The labour-intensive mechanical removing method is not practical in large areas, with chemical herbicides being used instead. Although this method is more effective than the mechanical process, its side effects need to be considered.

To minimise the potentially harmful effects of the chemical and bacterial agents on the ecosystem, the method we propose is to create herbicide maps to map these regions of weeds more efficiently, systematically reducing the amount of herbicide required. The utilisation of standard spray sizes will assist with creating an effective and realistic model that can be generated to assist with the removal of weeds.

The identification and assessment of the invasive weeds' distribution are essential for management methods. Using a UAV for rapid airborne data acquisition from low altitudes and utilising online cloud services to perform machine learning techniques in identifying weed invasions is a fast and cost-effective approach. Unlike classical hand-crafted, feature-based detection techniques, the deep learning-based detection techniques can be retrained further with newly obtained data to improve its detection capability further.

5.3 Herbicide Accuracy

The herbicide accuracy is defined as the percentage of weeds which are in a spray region. The intersection of the Ground Truth (GT) with the herbicide map provides valuable information about whether weeds have been accounted for or not. True Positive (TP) is defined as weeds that intersect with the herbicide map, and False Negative (FN) is considered the symmetric difference of this value. This is demonstrated through the following equations:

$$TP_{H_j} = GT_j \cup H_{p_j} \qquad FN_{H_j} = GT_j \Delta H_{p_j} \tag{26}$$

The accuracy of the herbicide map then becomes the weeds which the herbicide map has detected, divided by

Figure 8: Herbicide Accuracy, Herbicide Saved and Herbicide Efficiency in order. H_p is the prediction herbicide mask, $!H_p$ is the inverse prediction mask, H_{GT} is the ground truth herbicide mask and GT is the original ground truth weed data.

the total amount of weeds. This is described in the following equation:

$$H_{acc} = \frac{TP_{H_j}}{TP_{H_j} + FN_{H_j}} \tag{27}$$

H_{acc} is the herbicide accuracy (%), H_p is the prediction herbicide mask, and j is the prediction image being used.

5.4 Herbicide Saved

The herbicide used by farmers in regular operation typically covers an entire field. Herbicide maps are used to reduce the amount of herbicide required, in doing so, decreasing the large monetary requirements of herbicides. The herbicide saved is equivalent to the total size of the area minus the weeds predicted. This is detailed in the following equation and demonstrated in Figure 8.

$$H_{sav} = 1 - \frac{H_{p_j}}{H_{p_j} + !H_{p_j}} \tag{28}$$

H_{sav} is the herbicide saved (%), H_p is the final prediction herbicide mask, and j is the prediction image.

5.5 Herbicide Efficiency

Herbicide saved is a quantitative term that does not declare whether an appropriate amount of herbicide was used or not. It is inefficient if a large portion of a field with little weeds is predominantly detected as a weed. Thus, the herbicide efficiency compares the predicted herbicide map to the ground truth herbicide map. The ground truth herbicide map, denoted as H_{GT}, is created using the same methods as the predicted data, as expressed in Section 5; however, using the original ground truth data instead. The intersection of H_{GT} with H_P is considered a TP and any symmetric difference between the two maps is a FN, as described through the following equations:

$$TP_{Hj} = H_{GT_j} \cup H_{p_j} \qquad FN_{Hj} = H_{GT_j} \Delta H_{p_j} \tag{29}$$

The efficiency of the herbicide map then becomes the regions that are shared by both H_{GT} and H_P over the total pixels in both regions:

$$H_{eff} = \frac{TP_{H_j}}{TP_{H_j} + FN_{H_j}} \tag{30}$$

The mean, represented by μ, of each metric, denoted as k (where k is H_{acc}, H_{eff} or H_{sav}), is used when extended over multiple images. i corresponds to the amount of prediction images which are being processed into herbicide maps.

$$\mu_k = \frac{1}{i} \sum_{j}^{i} (k) \tag{31}$$

5.6 Effective Spray Size

As spray size increased, the efficiency and accuracy improved, while herbicide saved decreased. A larger spray region means more potential weeds are detected within the region's bounds. Herbicide efficiency decreased during smaller spray sizes as less intersection between the prediction and ground truth herbicide maps are apparent.

The Euclidean distance between the herbicide saved and the accuracy and efficiency is independently calculated at each spray size, as expressed in Equation 32. The average between these two distances is used, and the minimum is selected from the range of sizes. This represents the most balanced spray size between saved herbicide, accuracy, and efficiency.

$$d^s_{avg} = \frac{(H^s_{eff} - H^s_{acc})^2 + (H^s_{eff} - H^s_{sav})^2}{2} \tag{32}$$

s is the spray size used, and d is the euclidean distance between two points. The most effective spray size is ≈ 0.45 m.

Prediction Results and Discussion

The herbicide maps generated between the ground truths and predictions of the *ResNet50-SegNet* model yield an accuracy of 84.51%, efficiency of 92.61% and 54.5% of herbicide saved.

The herbicide results are highly successful at optimising the semantic segmentation results, providing a method

Table 2: Herbicide saved using different flight paths

Flight ID	Name	Detection Characteristics	Herbicide Saved (%)
1	Backhouse	Predominantly large veins of capeweed	35.56
2	Shed Paddock	Consists of very large Scotch thistle clusters	56.65
3	Dam	Large Scotch thistle clusters, short capeweed veins, large regions of dirt	70.42
4	Vineyard Front	Limited spread of Paterson's curse, Scotch thistle and capeweed	81.96

of applying herbicide effectively and with increased accuracy. The herbicide saved overall images was 54.5%, implying that a farmer would have to pay for less than half of the originally required amount of herbicide. Compared to the semantic segmentation results in Table 1, the accuracy and efficiency of the herbicide map are significantly greater than the precision and F1-score of the semantic model. This represents the herbicide map optimising the prediction to detect an increased amount of weeds within input images.

Table 2 demonstrates that the system sufficiently saves a large majority of herbicide even though the characteristics of each region of land change. Previously, the results of the semantic segmentation only provided the ability to detect and classify weeds. The complete shape and size of the predictions did not match the GT data due to the imbalanced classes and labelling issues. The results of the herbicide mapping demonstrate that this metric evaluation is not necessary as long as the actual weed cluster can be identified. The herbicide mapping works purely from binary masks; thus, it can be extended to fit any prediction data and weed type. The robust nature of the algorithm allows it to increase the overall accuracy of semantic segmentation models effectively.

6 Frame Correlation and Geographical Mapping

An image database and flight log, as mentioned in Section 2, is provided from a generated flight path. To ensure flight log data is synchronised with imaging waypoints, only timestamps which feature a speed of 0 m/s are selected; these points being where the UAV stopped to take a picture. Each collected image is an input into the *ResNet50-SegNet* model, with the output being the semantic prediction of the weeds within the image. This image is processed through the procedures mentioned in Section 5 to produce an accurate herbicide map of the prediction image. The herbicide map generates an array of centroids and radiuses related to each weed. Using the transformation equation of the UAV with respect to objects, as mentioned in Equation 15, these centroids are converted to latitude, longitude and altitude points. These clusters of points are then mapped on a real world map, as demonstrated in Figure 9.

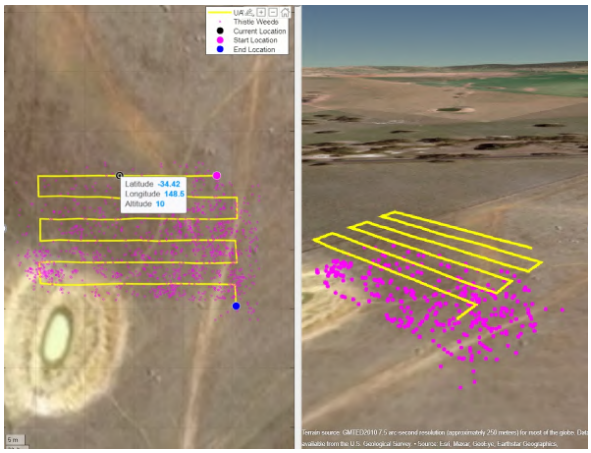

Figure 9: Pink dots represent the weeds, whilst the yellow lines are the UAV path on the geographic map

7 Conclusion and Future Work

This paper presented a method to detect, classify and map invasive weed species from UAV imagery. The proposed system successfully identifies the four weed classes of Scotch thistle, stinging nettle, capeweed and Paterson's curse. Detection and classification were achieved through the development of DL semantic segmentation models, which reduce unbalanced classes with loss functions. Mapping was performed by successfully calculating the path plans and transformations relative to the UAV. The implications of this paper provide farmers with the ability to perform SSWM through the creation of herbicide maps, minimising the amount of herbicide required and, by extension, associated environmental impacts. To our knowledge, this is the first research paper completed which extends semantic segmentation to provide a generalised output of weed locations instead of a pixel-perfect or direct-object detection region.

A unique attribute from this paper was how the herbicide maps were created using only prediction data. This enables the current system to be trialled on other weed detection networks, with the final goal being to create an algorithm that optimises commonly imbalanced and scarce weed datasets. Additionally, further research into the characteristic formations of weeds, such as clusters or veins, can potentially assist with herbicide map optimisation.

8 Acknowledgement

Thank you to Tristen Hobba, for assisting with the capturing and labeling of the UAV data.

References

[Asad and Bais, 2019] Muhammad Hamza Asad and Abdul Bais. Weed detection in canola fields using maximum likelihood classification and deep convolutional neural network. *Information Processing in Agriculture*, 2019.

[Briese, 2012] DT Briese. Onopordum acanthium l.–scotch thistle onopordum illyricum l.–illyrian thistle hybrids. *Julien, MH, McFadyen, R. & Cullen, J*, pages 416–424, 2012.

[Coleman *et al.*, 2018] Michael Coleman, Paul Kristiansen, Brian Sindel, and Christine Fyfe. Dwarf nettle (urtica urens): Weed management guide for australian vegetable production, 2018.

[Şafak Akıncı and Göktoğan, 2019] Şafak Akıncı and Ali Haydar Göktoğan. Detection and mapping of pine processionary moth nests in UAV imagery of pine forests using semantic segmentation. In *Australasian Conference on Robotics and Automation (ACRA-2019)*, page 9, Adelaide, Australia, Dec 2019.

[Göktoğan and Sukkarieh, 2015] Ali Haydar Göktoğan and Salah Sukkarieh. *Autonomous Remote Sensing of Invasive Species from Robotic Aircraft*, pages 2813–2834. Springer Netherlands, Dordrecht, 2015.

[Göktoğan *et al.*, 2010] Ali Haydar Göktoğan, Salah Sukkarieh, Mitch Bryson, Jeremy Randle, Todd Lupton, and Calvin Hung. A rotary-wing unmanned air vehicle for aquatic weed surveillance and management. *Journal of Intelligent and Robotic Systems*, 57(1):467–484, 2010.

[Heap and Trengove, 2008] John Heap and Sam Trengove. International research review: Site specific weed management. *Australian Grain*, 18(3):26–28, 2008.

[Jensen *et al.*, 2013] P. Jensen, I. Lund, and D. Nuyttens. Spray liquid distribution and biological efficacy of commercially available nozzles used for precision weed control. *Biosystems Engineering*, 116:316–325, 2013.

[Lin *et al.*, 2017] Tsung-Yi Lin, Priya Goyal, Ross Girshick, Kaiming He, and Piotr Dollár. Focal loss for dense object detection. In *Proceedings of the IEEE international conference on computer vision*, pages 2980–2988, 2017.

[Llewellyn *et al.*, 2016] R Llewellyn, D Ronning, M Clarke, A Mayfield, S Walker, and J Ouzman. Impact of weeds in australian grain production. *Canberra, ACT, Australia: Grains Research and Development Corporation*, 2016.

[Louargant *et al.*, 2017] M Louargant, S Villette, G Jones, N Vigneau, J N Paoli, and C Gée. Weed detection by uav: simulation of the impact of spectral mixing in multispectral images, 2017.

[McLeod, 2018] Ross McLeod. *Annual Costs of Weeds in Australia.* Centre for Invasive Species Solutions, November 2018.

[Milioto *et al.*, 2017] Andres Milioto, Philipp Lottes, and Cyrill Stachniss. Real-time semantic segmentation of crop and weed for precision agriculture robots leveraging background knowledge in cnns. *https://arxiv.org/abs/1709.06764*, 09 2017.

[Pflanz *et al.*, 2018] Michael Pflanz, Henning Nordmeyer, and Michael Schirrmann. Weed mapping with uas imagery and a bag of visual words based image classifier. *Remote Sensing*, 10(10), 2018.

[Rasmussen *et al.*, 2019] J Rasmussen, J Nielsen, J C Streibig, J E Jensen, K S Pedersen, and S I Olsen. Preharvest weed mapping of cirsium arvense in wheat and barley with off-the-shelf uavs. *Precision agriculture*, 20(5):983–999, 2019.

[Sa *et al.*, 2018] Inkyu Sa, Marija Popovic, Raghav Khanna, Zetao Chen, Philipp Lottes, Frank Liebisch, Juan I. Nieto, Cyrill Stachniss, and Roland Siegwart. Weedmap: A large-scale semantic weed mapping framework using aerial multispectral imaging and deep neural network for precision farming. *CoRR*, abs/1808.00100, 2018.

[Shaw, 2005] David Shaw. Remote sensing and site-specific weed management. *Frontiers in Ecology and the Environment*, 3:526, 12 2005.

[Sheppard and Smyth, 2012] Andy W Sheppard and Matthew Smyth. Echium plantagineum l.–paterson's curse. *Biological Control of Weeds in Australia*, pages 211–226, 2012.

[Tan and Li, 2019] Yumin Tan and Yunxin Li. Uav photogrammetry-based 3d road distress detection. *ISPRS International Journal of Geo-Information*, 8:409, 09 2019.

[Tian *et al.*, 2000] L.F. Tian, John Reid, and John Hummel. Development of a precision sprayer for site-specific weed management. *Transactions of the American Society of Agricultural Engineers*, 42, 03 2000.

[Wu *et al.*, 2019] W Wu, D Dawson, D Fleming-Muñoz, E Schleiger, and J Horton. The future of australia's agricultural workforce. *CSIRO Data61, Canberra. Centre for Social Research & Methods*, 61(2):6125, 2019.

[Zhang *et al.*, 2017] Airong Zhang, Isaac Baker, Emma Jakku, and Rick Llewellyn. Accelerating precision agriculture to decision agriculture: The needs and drivers for the present and future of digital agriculture in australia. 2017.